Flaw sensitivity in rate-sensitive high strength alloys: an assessment and future research directions

Suman Guha, Vikram Deshpande and Norman Fleck*

Cambridge University Engineering Dept., Trumpington St.,

Cambridge, CB2 1PZ, UK

* Corresponding author. E-mail address: NAF1@eng.cam.ac.uk

22 September 2016

Keywords: cleavage, short crack, rate sensitivity, transition flaw size

Abstract

The tensile strength of metallic alloys may be sensitive to the presence of short cracks, particularly in the embrittled state (such as phosphorous or sulphur segregation to the grain boundaries in a high strength steel). Experimental evidence reveals that cleavage accompanied by plasticity can occur when the net section stress is on the order of the yield strength. If the solid were mildly strain hardening but rate-insensitive, then no cleavage would be predicted as the crack tip tensile stress would not attain the local cleavage value. In the present study, the role of rate sensitivity is assessed by placing a tensile cohesive zone at the tip of an edge crack within a visco-plastic solid, and the crack is subjected to remote tension. Thereby, crack initiation and growth is predicted from short flaws in the presence of bulk plasticity. The crack growth resistance curve for long flaws is also determined. Implications of the predictions are discussed for hydrogen embrittlement, and the significance of rate effects in elevating the stress level adjacent to the crack tip is quantified.

1 Introduction

High strength alloys, in the presence of an embrittling species such as hydrogen, commonly fail by a combination of grain boundary cleavage and local plasticity. The grain boundary flaws that initiate such failure are often sub-micron in length, see for example Wang et al [1-3]. This raises the question: how can the stress level ahead of a small flaw, and in the

presence of plastic flow, be sufficient to overcome the cleavage strength? One suggestion is that plastic strain gradients are extremely high near the tip of a flaw and these elevate dislocation density and local strength to levels on the order of the cleavage strength [4]. An alternative explanation is that material strain rate sensitivity, in combination with high strain rates at the tip of a flaw, lead to stress levels in excess of the cleavage strength. We shall explore the implications of this second explanation in the current study.

The flaws triggering cleavage in a hydrogen-embrittled steel are remarkably small in comparison to the crack tip plastic zone size for a long crack in the embrittled state. This implies that a plastic field surrounds the short cracks, with no K field present. This will be discussed in the context of the present study and of the literature in the discussion section below.

Our study builds on the pioneering work of Tvergaard and Hutchinson [5] and the more recent study of Landis et al [6]. Both studies addressed the problem of crack growth from the cohesive zone at the tip of a long crack within an elasto-plastic solid of yield strength σ_Y and selected levels of strain hardening. Tvergaard and Hutchinson [5] predicted the crack growth resistance curve, the so-called R-curve, for a long crack by assuming a tensile cohesive zone of peak strength $\sigma_{\max}$ and of toughness Γ_0 (equal to the area under traction versus separation curve). The initiation toughness K_0 for the onset of crack growth follows directly from the Irwin relation $E\Gamma_0 / \left(1-\nu^2\right) = {K_0}^2$ in terms of the Young's modulus E and Poisson ratio ν.

Tvergaard and Hutchinson [5] predicted the R-curve for a long crack, including the steady state value of stress intensity factor K_{ss} for extended crack growth. For example, for mild strain hardening, they showed that K_{ss}/K_0 increases dramatically with increasing $\sigma_{\max}/\sigma_Y$ in the vicinity of $\sigma_{\max}/\sigma_Y = 3$. The mechanistic explanation is as follows. The maximum traction ahead of the crack tip in an elastic, ideally-plastic solid is given by the Prandtl field $T \approx 3\sigma_Y$, and this value changes only slightly with crack advance. A tensile traction of this magnitude is insufficient to overcome the cohesive strength $\sigma_{\max}$ when $\sigma_{\max}/\sigma_Y > 3$: neither crack initiation nor crack growth can occur. This restriction is relaxed for a rate-sensitive solid: high strain rates at the crack tip can generate tractions that exceed

$3\sigma_Y$ and thereby overcome the cohesive strength $\sigma_{\max}$. This case was considered by Landis et al [6]. They determined the limiting value K_{ss}/K_0 for imposed crack growth rates $\dot{a}$ rather than the full R-curve, and they found that K_{ss}/K_0 decreases with increasing $\dot{a}$.

Experiments on unnotched specimens made from hydrogen-charged, high strength steels reveal that cleavage can occur at an applied stress comparable to the yield strength [1-3]. The study of Landis et al. [6] suggests that strain rate sensitivity may be the source of the high tensile stresses at the tip of a short defect to trigger cleavage. This motivates the present study. The growth of short and long cracks in a rate-sensitive solid is addressed, with the aim of exploring the effect of strain rate upon the cleavage strength of a metallic solid in the presence of visco-plasticity.

2 Description of numerical model

We shall analyse crack growth in an edge-cracked specimen loaded in uniaxial tension, as sketched in Fig. 1a. The solid satisfies J2 rate dependent plasticity and crack growth is modelled by a cohesive zone law. The plane strain problem is analysed in a small strain setting with the following boundary conditions. The edge crack is perpendicular to the edge of the specimen and symmetry dictates that only the upper half of the specimen needs to be analysed, such that the analysed domain occupies $0 \le x_1 \le W$ and $0 \le x_2 \le H$; the specimen is loaded in uniaxial tension along the x_2 direction. Symmetry along the $x_2 = 0$ boundary also implies that the shear traction vanishes, $T_1 = 0$, over $0 \le x_1 \le W$. The initial crack tip is located at $x_1 = a_0$, such that the tensile traction T_2 vanishes over the crack flank $0 < x_1 < a_0$. A cohesive surface is placed ahead of the crack on $a \le x_1 \le W$ in order to model mode I crack extension.

2.1 *Material model*

An isotropic elasto-viscoplastic formulation is adopted, such that the total strain rate $\dot{\varepsilon}_{ij}$ is the sum of elastic and plastic strain rates, $\dot{\varepsilon}^e_{ij}$ and $\dot{\varepsilon}^p_{ij}$, respectively. The elastic strain is related to stress via the isotropic Hooke's law as characterised by the Young's modulus E and Poisson's ratio ν. The plastic strain rates satisfy [6]

$$\dot{\varepsilon}_{ij}^{p} = \frac{3}{2}\,\dot{\varepsilon}_0 \left(\frac{\sigma_e}{\sigma_0}\right)^{\frac{1}{m}} \frac{s_{ij}}{\sigma_e}, \tag{2.1}$$

where s_{ij} is the deviatoric stress and σ_e is the von-Mises equivalent stress, while σ_0, $\dot{\varepsilon}_0$ and m are the reference strength (ie flow strength), reference strain rate and strain rate exponent, respectively.

Crack growth is modeled through a cohesive traction versus displacement relation. Since crack growth occurs on the symmetry plane $x_2 = 0$ it suffices to specify a relation for the normal traction T_2 and crack opening Δ_2 such that

$$T_2 = -e\frac{\Delta_2}{\delta_n}\sigma_{max} exp\left(-\frac{\Delta_2}{\delta_n}\right), \tag{2.2}$$

where σ_{max} is the peak crack opening traction that occurs at an opening $\Delta_2 = \delta_n$, and the fracture energy is $\Gamma_0 = e\sigma_{max}\delta_n$. The crack opening Δ_2 is related directly to the material displacement along the bottom face of the specimen in Fig. 1a, such that $\Delta_2 = 2u_2(x_1, 0)$. Under plane strain conditions, crack growth in an elastic solid occurs when the applied mode I stress-intensity factor attains the value

$$K_0 \equiv \sqrt{\frac{E\Gamma_0}{1-\nu^2}}. \tag{2.3}$$

The results presented below are for a specimen with $H/W = 4$ and $a_0/W = 0.1$, and for a solid with yield strain $\varepsilon_0 = \sigma_0 / E = 0.003$, Poisson's ratio ν =0.3 and strain rate sensitivity exponent $m = 0.1$.

2.1 Numerical method

The boundary value problem is solved using the finite element method. The domain is meshed using constant strain triangular elements. A representative value for the length of the cohesive process zone length is specified by the Dugdale plastic zone length [7]

$$l_c = \frac{\pi}{8}\frac{E\Gamma_0}{\sigma_{max}^2}. \qquad (2.3)$$

To ensure adequate mesh resolution, the finite element mesh size l_e near the crack tip is taken to satisfy the requirement $l_c/l_e \geq 20$ in all calculations. Unless otherwise stated, results are given for a short crack ($a_0/\delta_n = 50$) and for a long crack ($a_0/\delta_n = 2.5 \times 10^4$).

The boundary value problem under consideration is uniaxial tension of the edge cracked specimen. Numerical difficulties were encountered when uniaxial tension was imposed by specifying either a remote displacement $\overline{U}$ or remote stress σ_R on the boundary $x_2 = H$ in the x_2-direction. Neither method gave a monotonically increasing crack tip opening displacement due to the feature that the traction-displacement law has a softening portion. Additionally, a snap-back response is observed in the load versus remote displacement response for a long initial crack. To avoid both numerical difficulties a modified Ritz method was employed, as introduced by Tvergaard [8] and Lemonds and Needleman [9]), see Appendix A for details. In brief, the equilibrium response is determined for *a prescribed crack tip displacement rate* $\dot{\delta}_T$ while maintaining a spatially uniform displacement $u_2(x_1, H) = \overline{U}$ on the boundary $x_2 = H$. We emphasise that $\delta_T \equiv 2u_2(a_0, 0)$ is the opening at the initial crack tip. The remote displacement rate $\dot{\overline{U}}$ is adjusted such that the required crack tip opening rate $\dot{\delta}_T$ is achieved. This loading method could also be achieved experimentally, for example by performing a test with a crack tip clip gauge under feedback displacement control in a servo-hydraulic test machine. With the crack tip displacement rate $\dot{\delta}_T$ prescribed, the remote stress σ_R versus remote displacement $\overline{U}$ and the crack extension Δa are outputs from the model.

2.2 Non-dimensional groups

The non-dimensional crack tip opening displacement rate reads $\bar{\delta} \equiv \dot{\delta}_T/(a_0\, \dot{\varepsilon}_0)$, where $\dot{\delta}_T$ is the crack tip opening displacement rate. This loading is maintained by applying a remote displacement $\overline{U}$ corresponding to an applied strain $\bar{\varepsilon} \equiv \overline{U}/H$ and a normalised strain rate $\dot{\bar{\varepsilon}}/\dot{\varepsilon}_0 \equiv \dot{\overline{U}}/(H\dot{\varepsilon}_0)$. The applied stress σ_R is work conjugate to $\bar{\varepsilon}$, and is written in non-dimensional form as $\bar{\sigma}_R \equiv \sigma_R/\sigma_0$. Define the current location x_{tip} of the crack tip as the

location on the cohesive surface for which $u_2 = 4\delta_n$, thereby defining the crack extension as $\Delta a = x_{tip} - a_0$.

The parameters varied in this study are the normalised cohesive strength σ_{max}/σ_0, the applied crack tip opening displacement rate $\bar{\dot{\delta}}$ and the initial crack length a_0/δ_n. In the long-crack limit ($a_0/\delta_n \to \infty$), small-scale yielding prevails and the applied loading is described in terms of the applied mode I stress intensity factor $K_I = Y\sigma_R\sqrt{\pi a}$ where a is the current crack length and Y is the stress-intensity calibration factor for the edge-crack geometry. At small values of a_0/δ_n large scale plastic yielding may occur prior to crack growth and K_I is not a valid loading parameter for the crack: the remote applied stress is then used to characterise the loading on the specimen. Unless otherwise stated, results are presented for $\sigma_{max}/\sigma_0 = 4$ and $\overline{\dot{\delta}} = 4$.

3 Results

Typical plots of the predicted responses are given in Fig. 2 for a short crack ($a_0/\delta_n = 50$) and for a long crack ($a_0/\delta_n = 2.5 \times 10^4$), with $\bar{\dot{\delta}} = 4$. The remote tensile stress $\bar{\sigma}_R$ versus normalised remote displacement, $\bar{\varepsilon} \equiv \bar{U}/H$ is plotted in Fig. 2a for both the short and long cracks, with $\sigma_{max}/\sigma_0 = 4$. A sharp snap-back in response accompanies crack growth for the long crack (see insert to the figure), whereas a peak load but no snap-back is observed for the short crack: the response is stable under increasing remote displacement but not under increasing remote load. We further note that the peak load in the presence of a short crack is close to the uniaxial strength absent a crack (at a remote strain rate of $\bar{\dot{\varepsilon}} = 2\dot{\varepsilon}_0$).

Representative R-curves for the long crack are plotted in Fig. 2b for selected values of σ_{max}/σ_0. The R-curve is sensitive to the magnitude of σ_{max}/σ_0 in a similar manner to that observed by Landis et al. [6] for the sensitivity of K_{ss}/K_0 to σ_{max}/σ_0. But a new feature emerges: at $\sigma_{max}/\sigma_0 = 3$, the K-resistance curve increases monotonically to K_{SS} with crack extension, whereas higher values of $\sigma_{max}/\sigma_0 = 4$ and 5 lead to a peak in K_R followed by a drop to K_{SS}. This K-transient is reflected by the evolution of active plastic zone with crack extension, compare Fig. 3a for σ_{max}/σ_0=3 with Fig. 3b for σ_{max}/σ_0=4. We note that the plastic zone has a pronounced peak in height after a small initial increment in crack growth for

$\sigma_{max}/\sigma_0 = 4$ but not for $\sigma_{max}/\sigma_0 = 3$. We emphasise that the K-resistance curves have been generated for a constant value of crack tip opening rate rather than for a constant crack velocity. The dependence of crack extension upon crack tip opening is shown in Fig. 2c; it is clear that the crack growth accelerates in all cases. This is made explicit by plotting in Fig. 2d the instantaneous crack velocity $\dot{a}$ as a function of crack tip opening δ_T (which is proportional to time). We deduce that the different shapes of R-curve in Fig. 2c cannot simply be explained in terms of accelerating crack growth rate.

A markedly different response is observed for a short crack, see Fig. 4 for the choice $a_0/\delta_n = 50$, with $\sigma_{\max}/\sigma_0 =$ 3, 4 or 5. The remote stress versus extension is plotted in Fig. 4a, and reveals that mild macroscopic softening accompanies crack extension. The peak normalised stress $\bar{\sigma}_f \equiv \sigma_f/\sigma_0$, where σ_f is the peak stress, is slightly above unity and is relatively insensitive to the value of σ_{max}/σ_0, in contrast to the R-curves of Fig. 2b. Also, the nominal strain of the specimen over the gauge length *H* of the edge-notched specimen is small, on the order of a few percent. Consequently, the specimen behaves in a quasi-brittle manner in a test involving an increasing load: the specimen fails catastrophically at a stress close to the yield strength of the unnotched specimen, and at low ductility.

The crack extension for the short crack much exceeds that for the long crack, at a given value of crack tip opening δ_T, compare Fig. 4b to Fig. 2c. Also, for the short crack, the crack extension increases in an almost linear manner with δ_T, implying that the crack growth rate $\dot{a}$ is almost constant. The nominal strain rate is plotted against crack tip opening (or equivalently against time) in Fig. 4c. For any prescribed value of σ_{max}/σ_0, the strain rate drops only by about a factor of about 2 during crack extension. Thus, in broad terms, the simulation of constant crack tip opening rate can be re-interpreted as a test where the applied strain rate is held approximately constant. As an example, if we assume $\dot{\varepsilon}_0 = 10^{-3}\text{s}^{-1}$ then the remote strain rates in Fig. 4c are of the order of magnitude as those in quasi-static tests.

The sensitivity of R-curve (for a long crack) and of strength (for a short crack) to the crack tip loading rate $\bar{\delta}$ is summarized in Figs. 5 and 6, respectively, for the selected case $\sigma_{max}/\sigma_0 = 4$. The R-curve drops and the crack velocity increases with increasing $\bar{\delta}$, see Fig. 5. This is consistent with the behaviour as noted by Landis et al. [6]: an increase in $\bar{\delta}$ elevates the crack tip stresses and the level of R-curve drops. In contrast, consider the short crack case,

see Fig. 6. The remote strain rate is almost constant and scales with $\bar{\delta}$, as shown in Fig. 6c. Consequently, the remote stress scales with $\bar{\delta}^m$ giving only a mild increase in strength of the specimen with increasing strain rate, see Fig. 6a. The crack velocity is almost constant in each simulation, but increases with increasing $\bar{\delta}$, as revealed in Fig. 6b.

The effect of crack length a_0 upon the non-dimensional gross section strength $\bar{\sigma}_f$ (that is, σ_f normalized by the flow strength σ_0) is shown in Fig. 7a for selected values of σ_{max}/σ_0, and a fixed crack tip opening rate $\bar{\delta} = 4$. The finite width of the specimen plays a negligible role as width W since it is held fixed at $W = 10a_0$. In similar manner, $\bar{\sigma}_f$ is plotted as a function of a_0/δ_n in Fig. 7b for selected values of $\bar{\delta}$ and $\sigma_{max}/\sigma_0 = 4$. A transition flaw size a_T can be identified for each of the curves, such that for $a_0 < a_T$, $\bar{\sigma}_f$ is almost independent of crack length, whereas for $a_0 \gg a_T$, $\bar{\sigma}_f$ scales with $K_{max}a_0^{-1/2}$ where K_{max} is the peak value of the R-curve. Then, in accordance with the usual prediction by linear elastic fracture mechanics, the transition flaw size reads $a_T = \frac{1}{\pi}\left(K_{\max}/\sigma_f\right)^2$.

Consider first the short crack response, such that $a_0 < a_T$. As noted previously in Fig. 4a, $\bar{\sigma}_f$ is close to unity, and relatively insensitive to the values of σ_{max}/σ_0 and of $\bar{\delta}$. The specimens fail in a quasi-brittle manner, with low ductility despite the fact that the cohesive zone strength much exceeds the flow strength: this behaviour is traced to the local elevation in strain rate at the crack tip, and consequently to a local elevation in traction on the cohesive zone, due to the rate dependence of the solid. A different sensitivity of $\bar{\sigma}_f$ to σ_{max}/σ_0 and to $\bar{\delta}$ is observed for a long crack, $a_0 >> a_T$. Specifically, $\bar{\sigma}_f$ increases with increasing σ_{max}/σ_0 and drops with increasing $\bar{\delta}$ at $a_0 \gg a_T$. This is consistent with the R-curve behaviour as shown in Figs. 2b and 5a for a long crack: the R-curve increases with increasing σ_{max}/σ_0 and drops with increasing $\bar{\delta}$. The normalised transition flaw size $a_T\varepsilon_0/\delta_n$ is plotted in Fig. 7c as a function of σ_{max}/σ_0 for selected values of $\bar{\delta}$. Consistent with the above discussion, a_T increases with increasing σ_{max}/σ_0 and with decreasing $\bar{\delta}$.

4. Implications for Hydrogen Embrittlement and some open questions

Hydrogen embrittlement is a pervasive problem particularly in the energy industry (oil, gas and nuclear), and is exacerbated by the increasing trend of using higher strength alloys, and protective coatings. For example, the interface between overlay welds or claddings and an underlying low alloy steel is prone to hydrogen embrittlement, particularly at carbides participates within the interfacial diffusion zone. Hydrogen embrittlement is also critical for welded joints since hydrogen take-up can arise from the use of damp electrodes in electric welding operations. There remains a need to develop a quantitative assessment methodology for hydrogen embrittlement, taking into account the effect of microstructure upon local diffusion of hydrogen, and the local strength and toughness of the material. Current engineering models are strength-based and account for size effects via Weibull theory, see for example [11,12].

A large number of theories of hydrogen embrittlement have been developed, but it has been difficult to gauge their accuracy due to a lack of precise test data on hydrogen concentration and due to a lack of detailed *quantitative* comparisons of measured and predicted strength for a range of specimen geometries and states of absorbed hydrogen, in a given material and heat treatment. A number of embrittlement mechanisms exist, with the dominant mechanism dependent upon microstructure, hydrogen concentration, temperature, and so on. However, inconsistencies in the predictive ability of current models have emerged recently, suggesting future directions in research. This is now explored in more detail.

It is generally recognised that high strength, tough steels, in the presence of hydrogen can cleave in a quasi-brittle manner from small flaws at a nominal tensile stress on the order of the yield stress. The present study gives a possible mechanistic explanation for this: rate sensitivity elevates the traction on small pre-existing flaws. But there remains an inconsistency. Material rate sensitivity increases the tendency for embrittlement at increasing macroscopic strain rates. In reality, hydrogen embrittlement is prevalent at low strain rates on the order of 10^{-5} s^{-1} and less so at higher strain rates on the order of $\dot{\varepsilon}_0 \approx 10^{-3}$ s^{-1}: embrittlement occurs as the strain rate is reduced, not increased. Some additional physics is required to explain this contradiction.

A fundamental mechanics-based understanding of the mechanics of hydrogen embrittlement remains elusive. Recently, Song and Curtin [13] have suggested that hydrogen embrittlement is closely linked to the prevention of crack tip blunting by dislocation emission

from the crack tip. They performed a molecular dynamics (MD) simulation of dislocation emission from a crack tip, with an outer imposed K field and no crack tip plasticity. They show that sufficient hydrogen at the crack tip allows for cleavage before dislocation emission. Dislocation emission blunts the crack tip and prevents crack growth.

Song and Curtin [12] consider a steel with a grain size on the order of 30 μm, and use their MD simulations to determine whether a flaw on the order of the grain size will lead to cleavage or crack tip blunting, see their Table 1. Their calculations suggest that the presence of hydrogen can lead to cleavage for such a flaw, and the associated threshold toughness is then inferred to be approximately 5 MPa $m^{1/2}$ for a steel of yield strength 500 MPa. However the measured values of threshold toughness for such steels is typically 20-60 MPa $m^{1/2}$. Furthermore, the high measured values of threshold toughness imply a large degree of crack tip blunting by dislocations in the vicinity of the crack tip: but these dislocations may not have nucleated from the crack tip. Conventional fracture mechanics suggests that the transition flaw for a steel of toughness 20-60 MPa $m^{1/2}$ and yield strength 500 MPa is on the order of $a_T = 0.2$mm, implying that a defect on the length of 30 μm has only a minor effect upon the strength. Again, it is clear that some additional physics is needed in order to understand cleavage in the presence of hydrogen.

5. Concluding Remarks

The present study suggests that cleavage from both short and long cracks in rate sensitive high strength metallic alloys is due to the fact that the stress level in the vicinity of a crack tip is elevated by high strain rates near the crack tip. There is a body of experimental evidence to suggest that fracture toughness drops with increasing loading rate, see for example Shoemaker and Rolfe [14]. At sufficiently low temperatures , ferritic steels fail by cleavage rather than micro-void coalesence. In that regime the toughness is seen to decrease with increasing loading rate in line with our predictions. Further work is needed however to explain fully the dependence of strength (and toughness) of steels after embrittlement by hydrogen.

6. Acknowledgements

The authors would like to acknowledge the funding and technical support from BP through the BP International Centre for Advanced Materials (BP-ICAM) which made this research possible. The authors are also grateful for funding in the form of an ERC advanced grant 669764, MULTILAT, and to the US Office of Naval Research N62909-14-1-N232, project managers Dr. David Shifler and Judah Goldwasser.

Appendix A. Loading by control of the crack tip opening displacement

The boundary value problem under consideration is uniaxial tension of the edge cracked specimen. Normally, such a boundary condition is imposed by specifying either a remote displacement $\overline{U}$ or remote stress σ_R on the boundary $x_2 = H$ in the x_2-direction. However, crack growth can result in snap back such that no equilibrium path exists for monotonically increasing $\overline{U}$ or σ_R. Thus, we chose to determine the equilibrium path for a specified monotonically increasing crack tip opening displacement $\delta_T = 2u_2(a_0, 0)$ using the Ritz type algorithm as introduced by Lemmonds and Needleman [9] while maintaining a spatially uniform displacement $u_2(x_1, H) = \overline{U}$ on the boundary $x_2 = H$. We prescribe $\dot{\delta}_T$ and ensure that the work conjugate force F_2 vanishes by employing a Rayleigh-Ritz method. The ermote displacement $\overline{U}$ becomes an outcome of the solution. Here, we briefly describe this algorithm.

We employ an elasto-viscoplastic constitutive relation. This rate dependent model is implemented in the FE formulation using the tangent modulus algorithm of Peirce et al. [10] with the stress rate $\dot{\sigma}_{ij}$ given in terms of the total strain rate $\dot{\varepsilon}_{ij}$ by

$$\dot{\sigma}_{ij} = L^{tan}_{ijkl}\dot{\varepsilon}_{kl} - \frac{\dot{\varepsilon}_t}{1+\xi} L_{ijkl}\left(\frac{3}{2}\frac{s_{kl}}{\sigma_e}\right) \qquad \text{(A1)}$$

where L_{ijkl} is the tensor of elastic moduli, L^{tan}_{ijkl} the tangent tensor as defined in Peirce et al. [10] and $\dot{\varepsilon}_t$ is the equivalent plastic strain rate at time t as given from Eq. (2.1) as $\dot{\varepsilon}_t \equiv \sqrt{(2/3)\dot{\varepsilon}^p_{ij}\dot{\varepsilon}^p_{ij}}$. The numerical parameter ξ depends on the choice of time integration scheme, as detailed in [10]. By employing (A1) in the finite element discretisation of the incremental principle of virtual work gives a system of equations

$$K_{ij}\dot{U}_j\delta\dot{U}_i = S_i\delta\dot{U}_i \qquad \text{(A2)}$$

where K_{ij} is the tangent stiffness matrix and the body force S_i results from the second term on the right hand side of Eq. (A1). The nodal velocities are then expressed as a combination of three sub-problems *m*=I, II and III,

$$\dot{U}_i = \sum_{m=I}^{III} w_m \, \dot{U}_i^{(m)} \tag{A3}$$

where w_m are co-efficients to be determined and the nodal velocities $\dot{U}_i^{(m)}$ are solutions to

$$K_{ij}\dot{U}_i^{(m)} = F_i^{(m)} \tag{A4}$$

in terms the right-hand side $F_i^{(m)}$ of the m^{th} sub-problem.

The three sub-problems for *m*=I, II and III are:

(I) A unit velocity $\dot{u}_2(x_1, H) = 1$ is prescribed on the top face of the specimen, $x_2 = H$, with the crack tip opening displacement restrained such that $\dot{u}_2(a_0, 0) = 0$ and body force $F_i^{(I)} = 0$.

(II) A opening displacement velocity $\dot{u}_2(a_0, 0) = \dot{\delta}_T$ is applied with $\dot{u}_2(x_1, H) = 0$ on the boundary $x_2 = H$ and body force $F_i^{(II)} = 0$. Here $\dot{\delta}_T$ is the imposed crack-tip opening displacement rate.

(III) A homogeneous set of boundary conditions with $\dot{u}_2(x_1, H) = 0$ on the boundary $x_2 = H$ as well as $\dot{u}_2(a_0, 0) = 0$ but body force $F_i^{(III)} = S_i$.

After the velocities associated with the three sub-problems have been computed, the three scalar weights w_m are determined as follows. Since the right hand term of Eq. (A1) only appears in sub-problem (III) we can readily show that $w_{III} = 1$ in order to satisfy the constitutive relation. Moreover, the crack tip opening is only imposed in sub-problem (II) and thus the weight $w_{II} = 1$. It now remains to determine $w_{(I)}$. Recall that the imposed loading is uniaxial tension with no external crack tip opening force. Thus, we require that the external force $F_2(x_1 = a_0, x_2 = 0) = 0$. Upon defining $F_2^{T(m)} \equiv F_2^{(m)}(x_1 = a_0, x_2 = 0)$ for sub-problem m we then impose

$$w_I F_2^{T(I)} + w_{II} F_2^{T(II)} + w_{III} F_2^{T(III)} = 0 \qquad \text{(A5)}$$

to obtain $w_{(I)}$.

References

1. Wang, M., Akiyama, E. and Tsuzaki, K., *Cross head speed dependence of the notch tensile strength of a high strength steel in the presence of hydrogen*. Scr. Mater., 2005. **53**(6): p. 713-718.

2. Wang, M., Akiyama, E. and Tsuzaki, K., *Effect of hydrogen and stress concentration on the notch tensile strength of AISI 4135 steel*, Mater. Sci. Eng., 2005. **A398** (1-2): p. 37-46.

3. Wang, M., Akiyama, E., Tsuzaki, K., *Effect of hydrogen on the fracture behaviour of high strength steel during slow strain rate test*. Corros. Sci., 2007. **49**(11), p. 4081-4097

4. Martínez-Pañeda, E., Niordson, C F. and Gangloff, R.P., *Stain gradient plasticity-based modelling of hydrogen environment assisted cracking*, Acta Materialia, 2016. **117**: p. 321-332.

5. Tvergaard, V., Hutchinson, J.W., *The relation between crack growth resistance and fracture process parameters in elastic-plastic solids*, J. Mech. Phys. Solids, 1992. **40**(6): p. 1377-1397.

6. Landis, C.M., Pardoen, T., Hutchinson, J.W., *Crack velocity dependent toughness in rate dependent materials*. Mech. Mater., 2000. **32**: p. 663-678.

7. Dugdale, D.S. (1960). *Yielding of steel sheets containing slits*. J. Mech. Phys. Solids, 1960. **8:** p. 100–104.

8. Tvergaard, V., *Buckling of elastic-plastic oval cylindrical shells under axial compression*, Int. J. Solids Struct. 1976. **12**, p. 683-691.

9. Lemonds, J., Needleman, A., *Finite element analyses of shear localization in rate and temperature dependent solids*, Mech. Mater. 1986. **5**: p. 339-361.

10. Peirce, D., Shih, C.F., Needleman, A., 1984. *A tangent modulus method for rate dependent solids*, Comput. Struct., 1984. **18**: 875-887.

11. Ayas, C., Deshpande, V.S. and Fleck, N.A., *A Fracture Criterion for the Notch Strength of High Strength Steels in the Presence of Hydrogen*. J. Mech. Phys. Solids, 2014. **63**: p. 80-93.

12. Ayas, C., Fleck, N.A. and Deshpande, V.S., *Hydrogen embrittlement of a biomaterial*, Mechanics of Materials, 2014. **80**: p.193-202.

13. Song, J. and Curtin., W.A., *Atomistic mechanism and prediction of hydrogen embrittlement in iron.* Nature materials, 2013. **12**: p. 145-151.

14. Shoemaker, A.K. and Rolfe, S.T., *The static and dynamic low temperature crack toughness performance of seven structural steels,* Eng. Fracture Mech., 1971. **2**: p. 319-339.

Figures

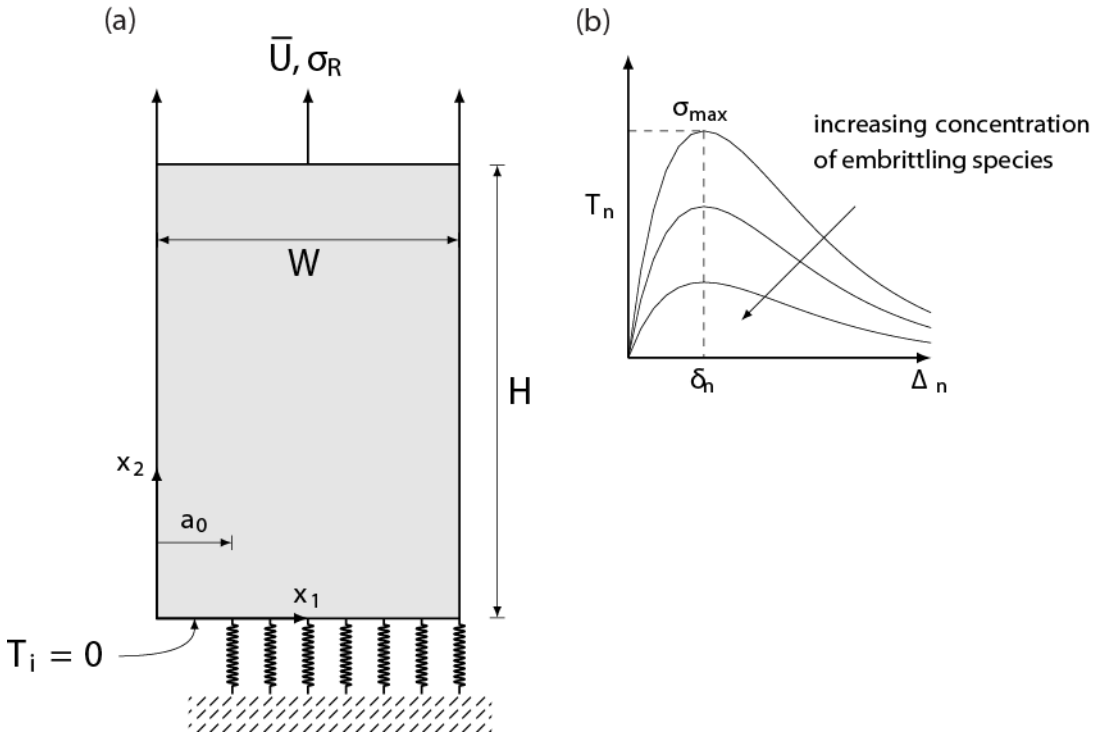

Figure 1. (a) Specimen geometry; (b) traction versus separation law of the cohesive zone.

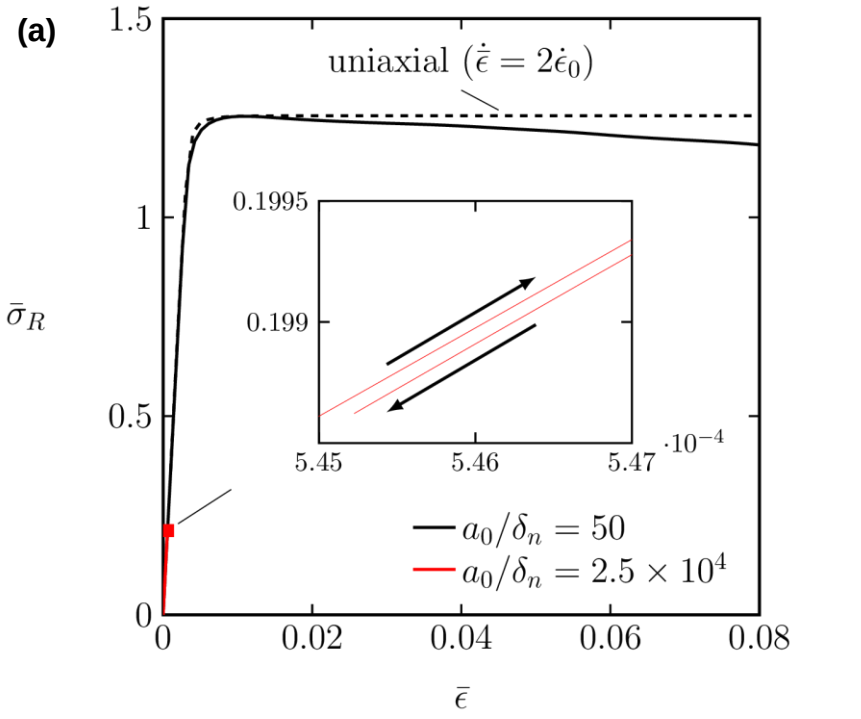
(a)
1.5
1
0.5
0
$\bar{\sigma}_R$
uniaxial ($\dot{\bar{\epsilon}} = 2\dot{\epsilon}_0$)
0.1995
0.199
5.45
5.46
5.47
$\cdot 10^{-4}$
$a_0/\delta_n = 50$
$a_0/\delta_n = 2.5 \times 10^4$
0
0.02
0.04
0.06
0.08
$\bar{\epsilon}$

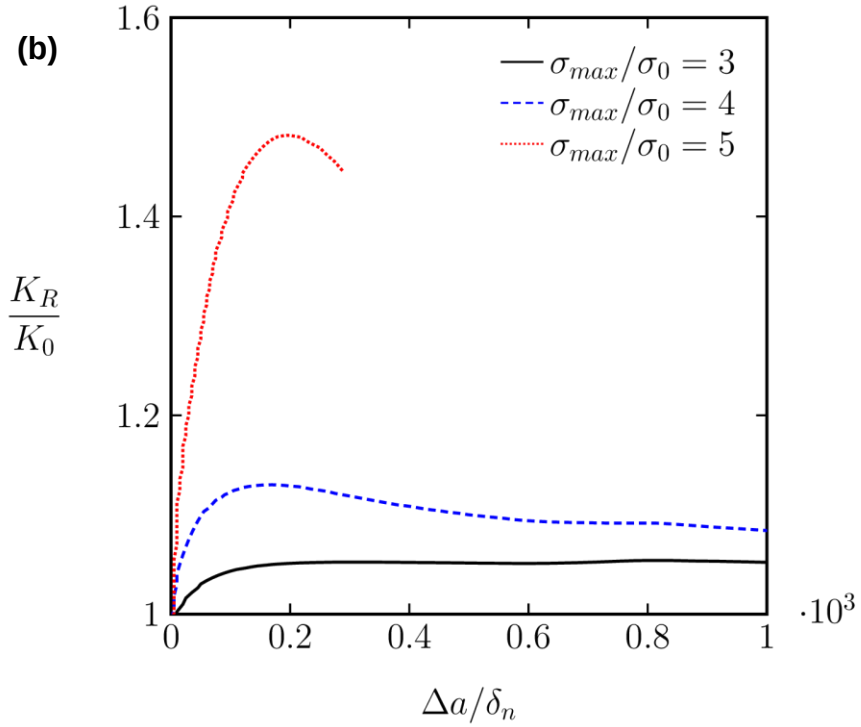
(b)
1.6
1.4
1.2
1
$\frac{K_R}{K_0}$
$\sigma_{max}/\sigma_0 = 3$
$\sigma_{max}/\sigma_0 = 4$
$\sigma_{max}/\sigma_0 = 5$
0
0.2
0.4
0.6
0.8
1
$\cdot 10^3$
$\Delta a/\delta_n$

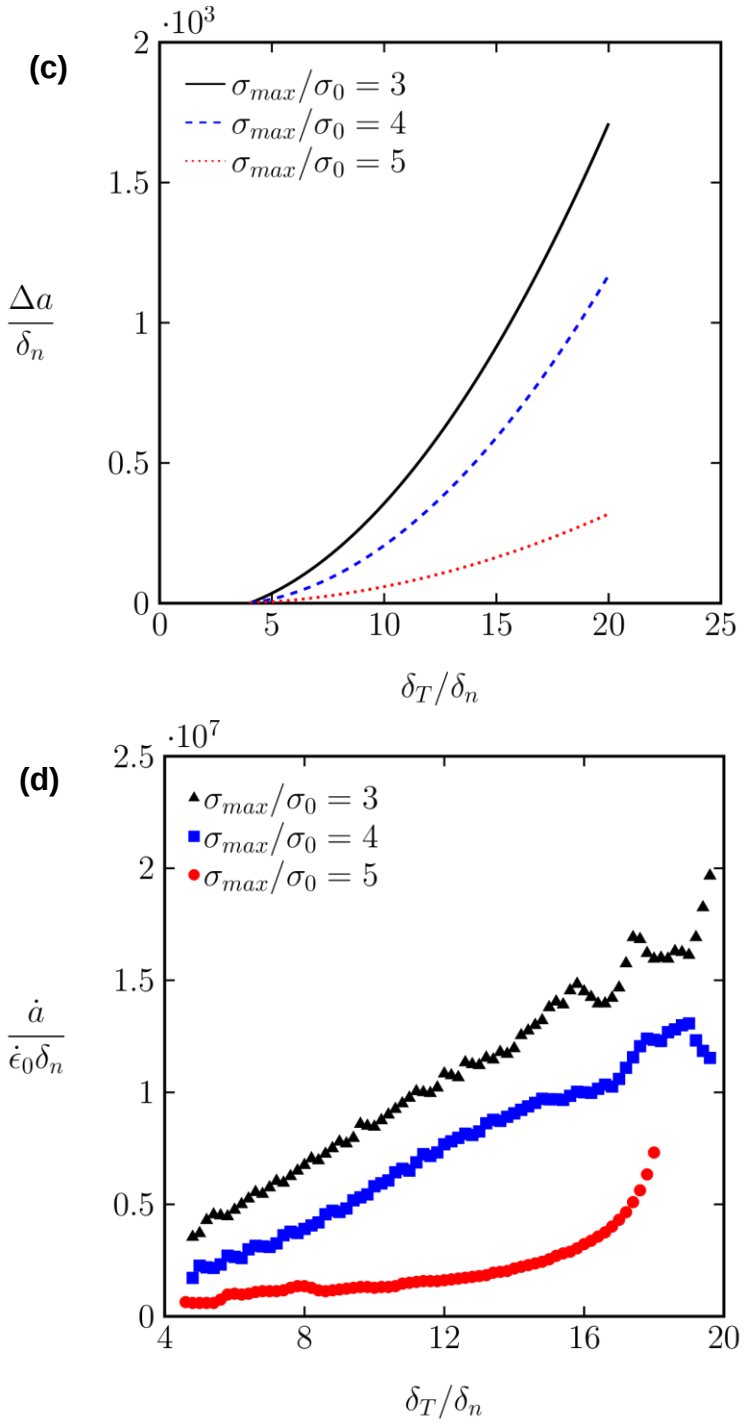

Figure 2. Crack growth predictions for a short crack $\left(\frac{a_0}{\delta_n} = 50\right)$ and for a long crack $(a_0/\delta_n = 2.5 \times 10^4)$, for $\overline{\delta} = 4$. (a) Average applied stress versus nominal strain for $\sigma_{max}/\sigma_0 = 4$. The arrows within the figure insert indicate loading and unloading of the long crack; (b) R-curves for a long crack, with selected values of σ_{max}/σ_0; (c) Crack growth and (d) crack velocity versus crack tip opening displacement at the initial crack tip for a long crack, with selected values of σ_{max}/σ_0. Crack velocities are calculated using a $O(h^4)$ central difference method from (c).

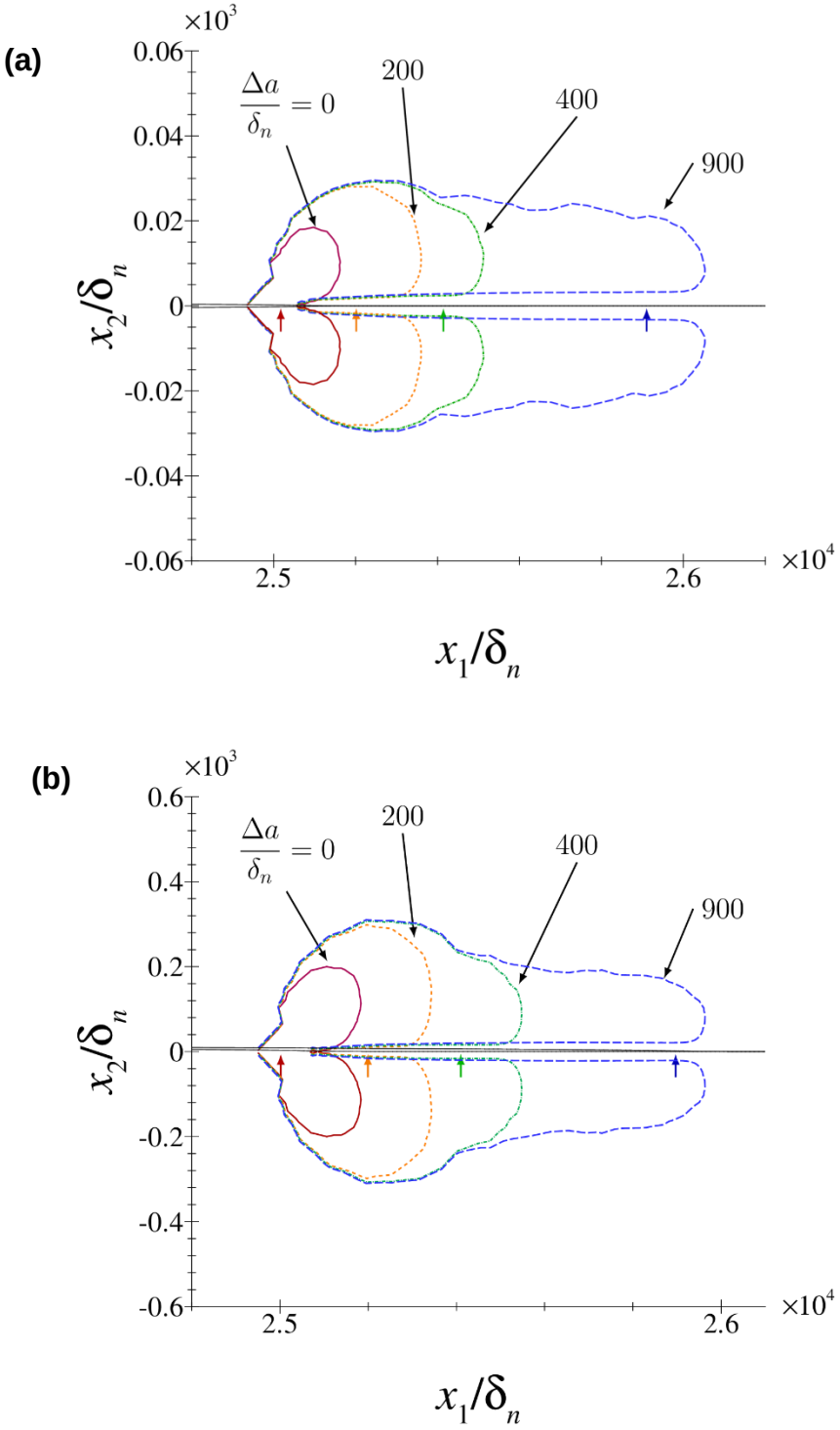

Figure 3. Contours of von Mises effective plastic strain ε_p for selected values of crack extension for a long crack ($a_0/\delta_n = 2.5 \times 10^4$) and $\overline{\delta} = 4$. (a) Contour $\varepsilon_p = 0.02\epsilon_0$ for a cohesive zone of strength $\sigma_{max}/\sigma_0 = 3$ and (b) contour of $\varepsilon_p = 0.2\epsilon_0$ for a cohesive zone of strength $\sigma_{max}/\sigma_0 = 4$. The arrows indicate the location of the current crack tip corresponding to the respective contours.

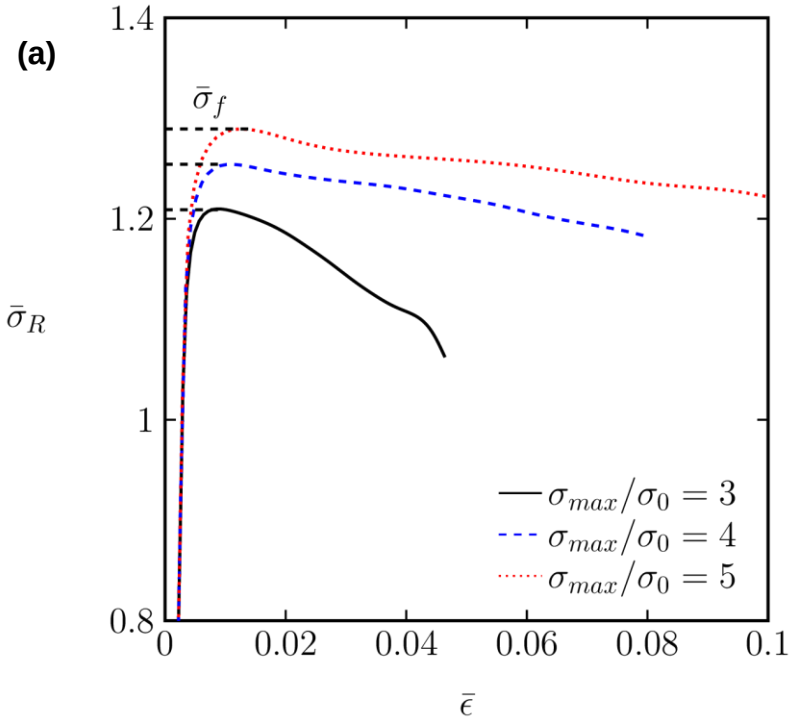
(a)
1.4
1.2
1
0.8
$\bar{\sigma}_f$
$\bar{\sigma}_R$
0
0.02
0.04
0.06
0.08
0.1
$\bar{\epsilon}$
$\sigma_{max}/\sigma_0 = 3$
$\sigma_{max}/\sigma_0 = 4$
$\sigma_{max}/\sigma_0 = 5$

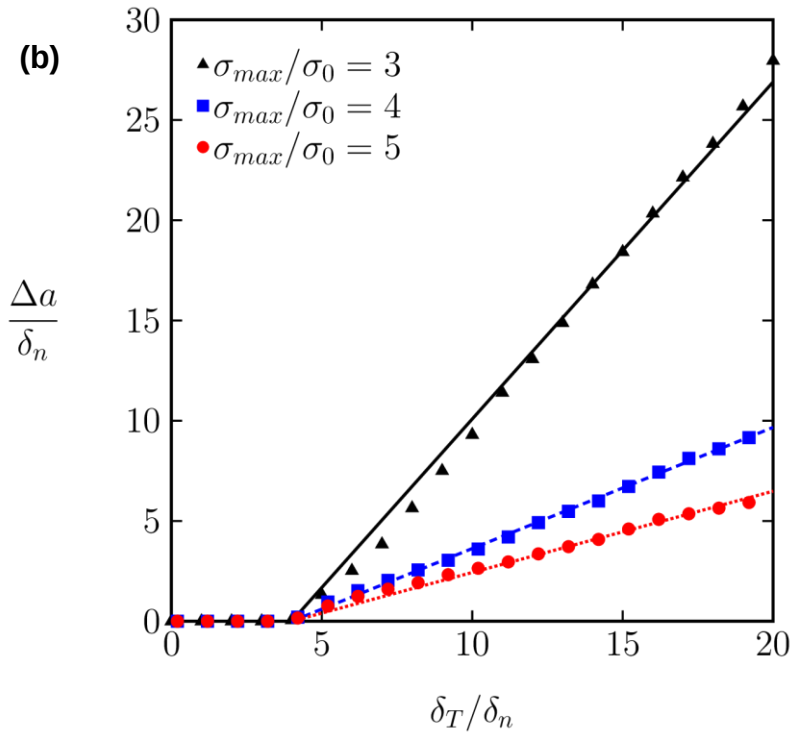
(b)
30
25
20
15
10
5
0
$\frac{\Delta a}{\delta_n}$
0
5
10
15
20
δ_T/δ_n
$\sigma_{max}/\sigma_0 = 3$
$\sigma_{max}/\sigma_0 = 4$
$\sigma_{max}/\sigma_0 = 5$

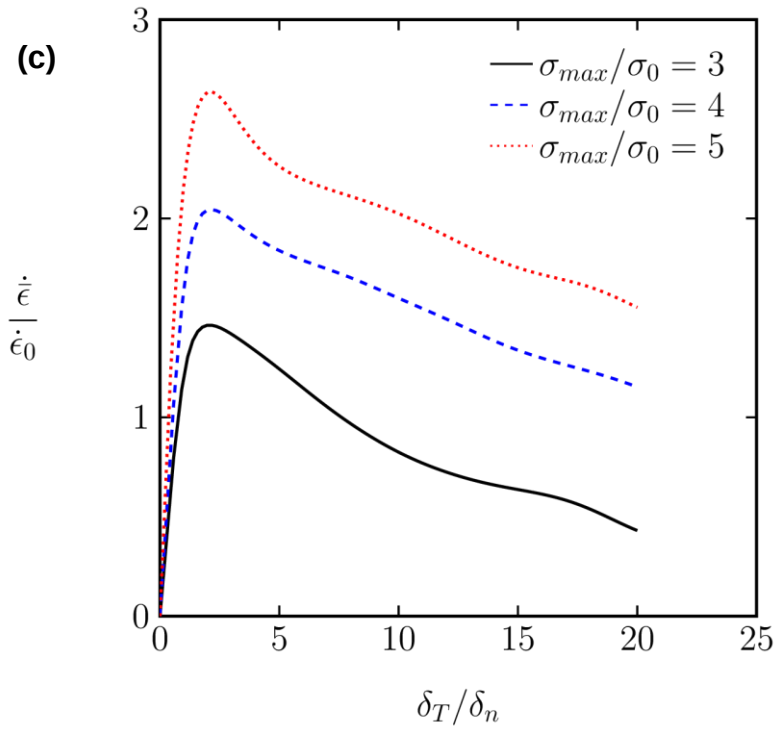

Figure 4. (a) Remote stress versus nominal strain, (b) crack growth versus crack tip opening displacement and (c) nominal strain rate for a short crack ($a_0/\delta_n = 50$). The crack tip opening displacement rate is $\overline{\delta} = 4$, and 3 selected values of cohesive strength are assumed, $\sigma_{\max}/\sigma_0 = 3, 4$ and 5.

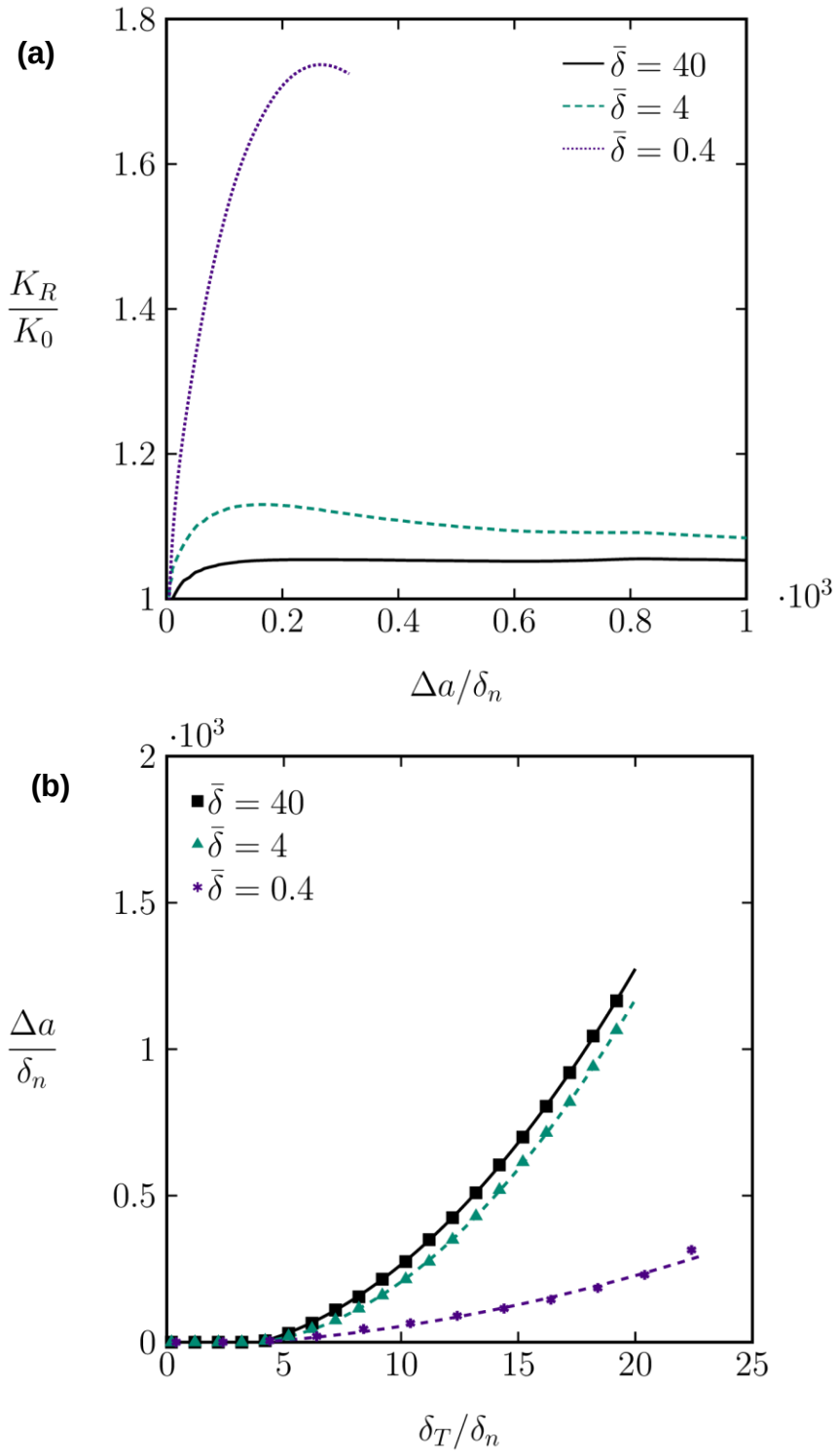

Figure 5. (a) R-curves and (b) crack growth versus crack tip opening displacement, for a long crack a_0 / δ_n =2.5x10^4 and $\sigma_{\max} / \sigma_0 = 4$, and for 3 values of $\bar{\delta}$.

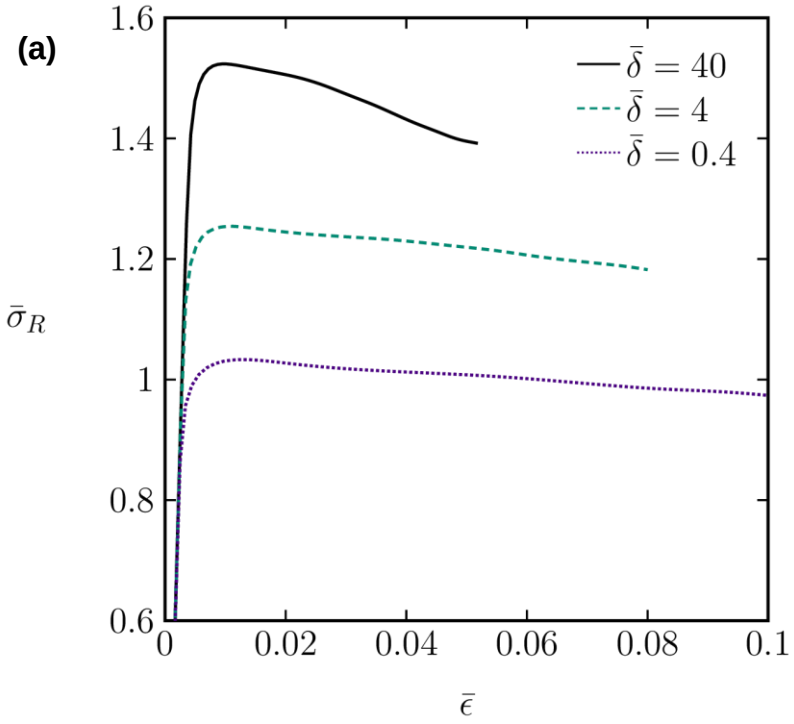
(a)
1.6
1.4
1.2
1
0.8
0.6
$\bar{\sigma}_R$
0
0.02
0.04
0.06
0.08
0.1
$\bar{\epsilon}$
$\bar{\delta} = 40$
$\bar{\delta} = 4$
$\bar{\delta} = 0.4$

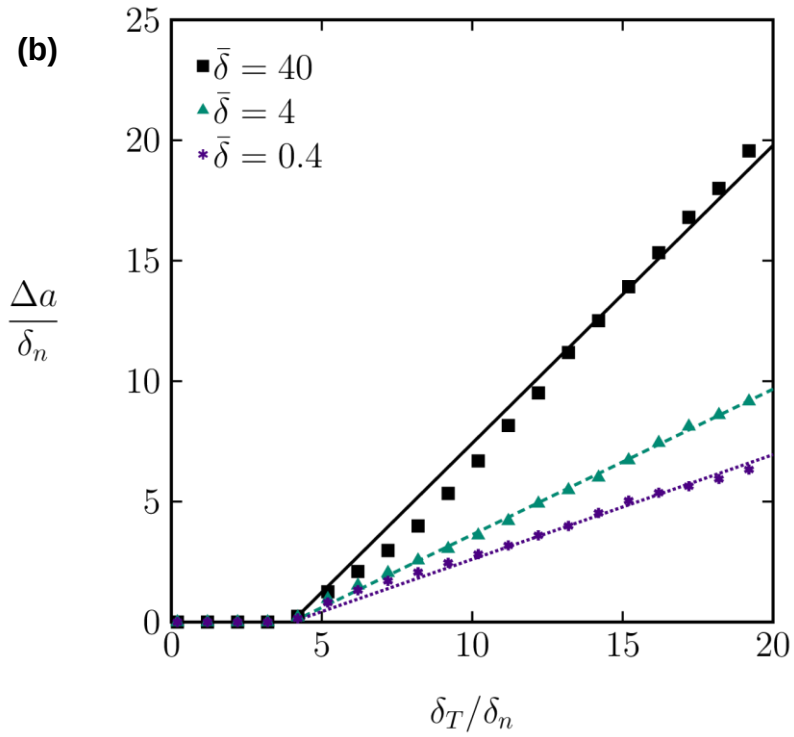
(b)
25
20
15
10
5
0
$\frac{\Delta a}{\delta_n}$
0
5
10
15
20
δ_T/δ_n
$\bar{\delta} = 40$
$\bar{\delta} = 4$
$\bar{\delta} = 0.4$

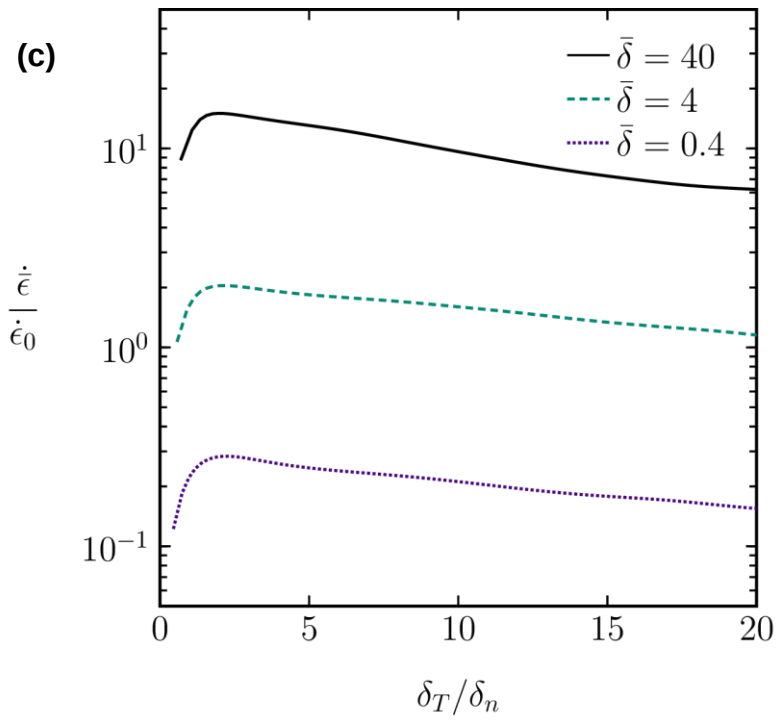

Figure 6. (a) Remote stress versus nominal strain; (b) crack growth versus crack tip opening displacement; and (c) nominal strain rate versus crack tip opening displacement for a short crack a_0 / δ_n =50 and $\sigma_{\max} / \sigma_0 = 4$.

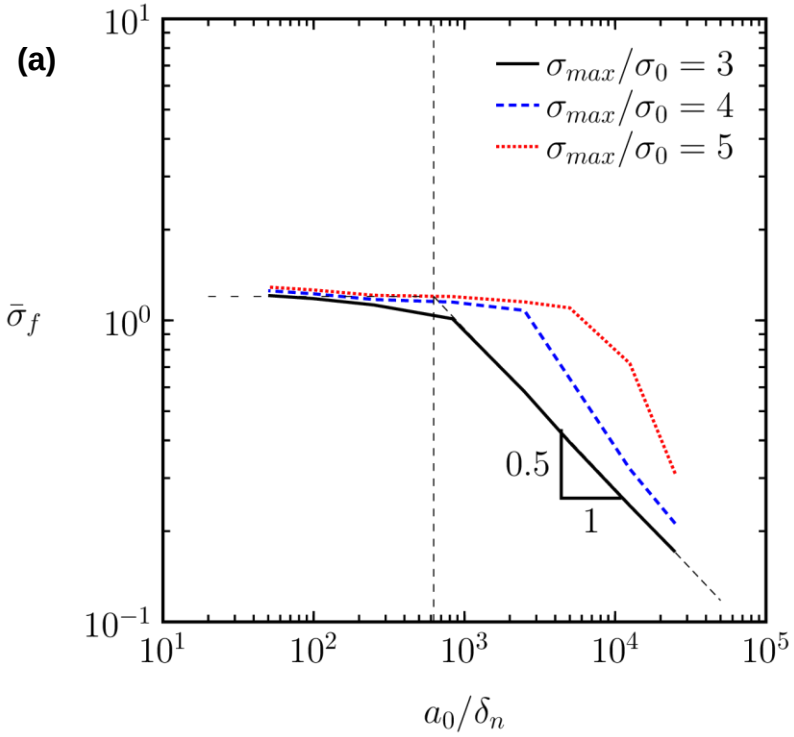
(a)
10^1
10^0
10^{-1}
$\bar{\sigma}_f$
$\sigma_{max}/\sigma_0 = 3$
$\sigma_{max}/\sigma_0 = 4$
$\sigma_{max}/\sigma_0 = 5$
0.5
1
10^1
10^2
10^3
10^4
10^5
a_0/δ_n

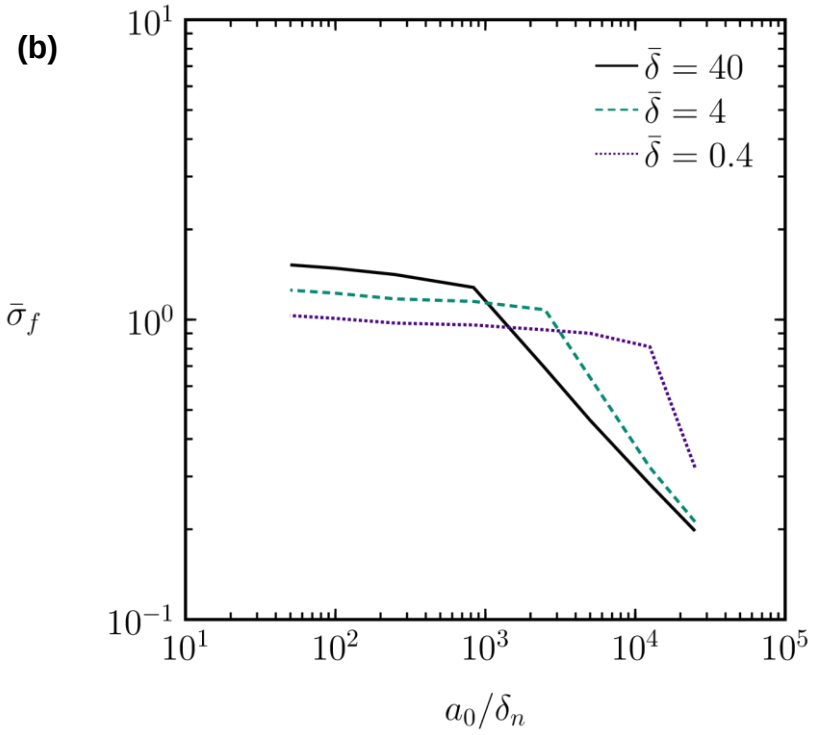
(b)
10^1
10^0
10^{-1}
$\bar{\sigma}_f$
$\bar{\delta} = 40$
$\bar{\delta} = 4$
$\bar{\delta} = 0.4$
10^1
10^2
10^3
10^4
10^5
a_0/δ_n

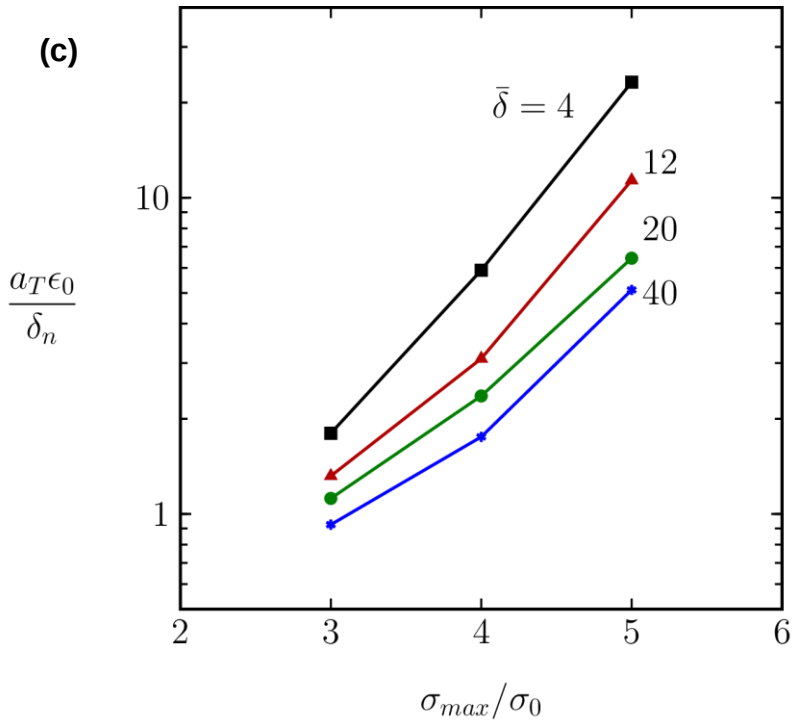

Figure 7. (a) Failure stress versus crack length for crack tip opening rate $\bar{\delta} = 4$ and for 3 values of cohesive zone strength $\sigma_{\max} / \sigma_0$; (b) failure stress versus crack length for $\sigma_{\max} / \sigma_0 = 4$ and for 3 values of $\bar{\delta}$; and (c) sensitivity of transition crack length to $\sigma_{\max} / \sigma_0$ for 3 values of $\bar{\delta}$, and for 3 values of $\sigma_{\max} / \sigma_0$.